Influence of Power Cycling Test Methodology on the Applicability of the Linear Damage Accumulation Rule for the Lifetime Estimation in Power Devices

Alessandro Vaccaro, *Student Member, IEEE*, and Paolo Magnone, *Senior Member, IEEE*

***Abstract*—The lifetime of power semiconductor devices, operating under a given mission profile and subjected to power cycling stress, is conventionally estimated under the assumption of linear damage accumulation rule, that is the application of the Miner's rule. To this purpose, lifetime models must be properly defined allowing to take into account for the relevant parameters of power cycling stress. This work shows how to estimate a cumulative distribution function in the case of an arbitrary temperature swing profile, starting from the statistical distribution at constant power cycling conditions. It is found that the accuracy of the linear damage accumulation rule is related to the experimental methodology adopted for power cycling tests. A detailed experimental activity is carried out on packaged insulated gate bipolar transistor (IGBT) devices, providing useful guidelines for the definition of lifetime models to be adopted in the Miner's rule.**

***Index Terms*—Insulated gate bipolar transistors, lifetime estimation, power cycling, power semiconductore devices, semiconductor device reliability.**

I. Introduction

THE application of power devices in the industrial and automotive fields requires the fulfillment of various specifications and standards related to the reliability of power semiconductor devices [1], [2]. The concept of analyzing the reliability of power devices is fundamental to obtaining an acceptable tradeoff between service costs and product costs [3].

There are several failure mechanisms affecting power systems that are being studied in the field of reliability, including the phenomenon of thermal/power cycling in semiconductor devices [4]. The physical degradation mechanism is related to the thermo-mechanical stress created at the interface of two materials with different coefficients of thermal expansion (CTEs) [5], [6], [7]. The wire bonds degradation is related to the different CTEs between Si and Al. The stress is then localized at the interface between materials and cracks are likely to be formed and to propagate in the aluminum wire [8]. In the case of aluminum reconstruction, thermo-mechanical stresses result in tensile stress at the metallization layer [9]. This type of process can exceed the elastic limits of the aluminum layer, leading to the formation of extrusion granules. In addition, the compressive stress, which is established at the aluminum/mold compound interface, induces a plastic behavior of the aluminum. As a result, an increase of series resistance can be observed [8]. The mismatch between the copper tab and the silicon die, which is a typical interface in discrete power devices, leads to the degradation of the solder joint with possible cohesion fracture or creep fatigue [10]. This type of degradation affects the thermal impedance of the component, since the heat dissipation takes place through the copper tab.

The above-mentioned degradation mechanisms are mainly triggered by the temperature cycling, but they are also affected by the average temperature and the heating time. Several models have been reported in literature, allowing to account for these parameters [11], [12], [13], [14], [15], [16], [17].

In general, there is a strong request for an accurate prediction of the lifetime in power electronics, in order to satisfy the reduction of development and testing time [18]. In a consolidated approach, the analysis of the reliability of a generic power system begins with the study of the mission profile [19], [20], [21]. Based on the electric and thermal models of the system, the mission profile is translated in a temperature profile in power semiconductor devices. The rainflow algorithm can be adopted to evaluate the number and the amplitude of temperature cycles [22]. Lifetime models are used to predict number of cycles to failure as a function of relevant parameters: temperature swing ΔT_j, minimum temperature $T_{j,\min}$, heating time $t_{\rm on}$, and current density per wire [5], [10], [11], [12], [14], [23]. The number of cycles to failure can be defined either as the average number or as the number leading to a given probability of failure (PoF). Hence, based on the considered lifetime model, Miner's rule is adopted to predict the lifetime consumption for a given temperature profile, under the assumption of linear damage accumulation (LDA). The applicability of LDA is a fundamental point, which have been considered in literature.

Manuscript received 19 December 2022; accepted 29 January 2023. Date of publication 6 February 2023; date of current version 10 March 2023. This work was supported in part by the research project "Interdisciplinary Strategy for the Development of Advanced Mechatronics Technologies (SISTEMA)," DTG, University of Padova-Project code CUP-C36C18000400001. Recommended for publication by Associate Editor W. Huang. *(Corresponding author: Paolo Magnone.)*

The authors are with the Department of Management and Engineering, Università degli Studi di Padova, 36100 Vicenza, Italy (e-mail: alessandro.vaccaro.1@studenti.unipd.it; paolo.magnone@unipd.it).

Color versions of one or more figures in this article are available at https://doi.org/10.1109/TPEL.2023.3242314.

Digital Object Identifier 10.1109/TPEL.2023.3242314

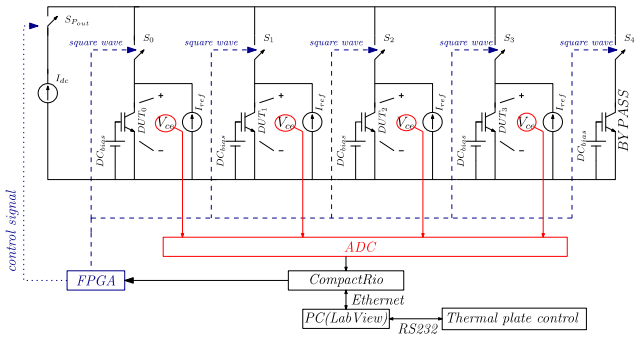

Fig. 1. Schematic of the setup adopted for power cycling tests. Four devices are tested simultaneously under the same stress conditions.

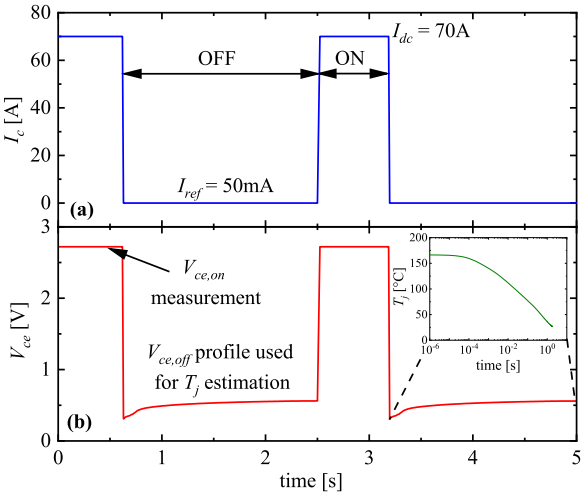

Fig. 2. Typical power cycling test. The current flowing in the DUT (a) is switched between a large value (ON phase) and a small value (OFF phase). The corresponding voltage drop is reported in (b). During the ON phase a large voltage drop is observed and the $V_{ce,\mathrm{on}}$ estimation is taken at the end of this phase. During the OFF phase, a sensing current (50 mA) is injected in the DUT and the $V_{ce,\mathrm{off}}$ profile is used for the estimation of T_j. The inset illustrates the temperature profile resulting from the application of the TSEP methodology to the $V_{ce,\mathrm{off}}$ profile.

In [21], LDA rule was validated considering the superimposition of different temperature profiles, having different heating times. Moreover, the analysis in [21] was carried out at different values of PoF. In [24], the application of combined power cycling stresses led to an underestimation in the lifetime prediction, which was explained assuming a dual degradation mechanism, resulting in a prediction error. In [25], under the assumption of a single degradation mechanism, combined power cycling stresses verified the applicability of LDA rule. In [26], combined experimental tests at different ΔT_j values did not verify the linearity of Miner's rule, particularly in the case of a combined stress with significantly different ΔT_j values (varying between 110 and 70 °C). In [27] and [28], the impact of combined vibrating and thermal cycling stresses was analyzed. An overestimation of the lifetime was found by applying Miner's rule. This inconsistency was ascribed to a change of the thermo-mechanical response due to the interaction between different types of stress [27] or to an additional stress phenomenon due to random vibrations during the test being temperature dependent [28]. In [29], a nonlinear cumulative damage model was proposed for ceramic column grid array electronic package subjected to a combination of thermal cycling and vibration. Also in [30], combined thermal cycling and vibration stress, under the assumption of a single failure mechanism, i.e., solder fatigue, led to an overestimation of lifetime with Miner's rule, because of dynamic effects combined with thermal stress. In [31], a nonlinearity in the accumulation of damage to solders in combined thermal cycling and vibration stress was found. In this case, the prediction error, despite the hypothesis of a single degradation mechanism and no interaction between the two stresses, was ascribed to the formation of intermetallic material at the interfaces or to the increase of voids size, amplifying the degradation process.

This work aims at extending a recent conference paper [32], in which the cumulative distribution function (CDF) was built up in the case of non-constant power cycling tests by means of Miner's rule and the results were compared with experiments. Different from [32], this work investigates how the power cycling test methodology affects the applicability of the linear damage accumulation rule. More specifically, power cycling tests are performed by following two different approaches:

1) "non-controlled ΔT_j" approach, in which a constant heating current is used to achieve the desired ΔT_j;
2) "active control of ΔT_j" approach, in which the heating time is modulated in order to keep the ΔT_j value close to the desired value for the entire experiment.

Therefore, this work investigates the influence of accelerated testing methodology on the lifetime estimation. Finally, compared to [32], the experimental activity is extended to different discrete power devices and with a larger records of test conditions.

The remainder of this article is organized as follows. Section II describes in detail the experimental setup adopted for power cycling tests, focusing on the different methodologies considered in the article. Section III reports the experimental results in the case of constant ΔT_j stress and in the case of an arbitrary profile of ΔT_j. In the latter case, experimental CDFs are compared with the predictions arising from the Miner's rule application. Finally, in Section IV, the main conclusions are summarized.

II. Experimental Setup and Power Cycling Tests

A. Experimental Setup

Power cycling experiments are performed by adopting a custom designed board, whose schematic representation is reported in Fig. 1. Four devices are stressed simultaneously under the same value of I_{dc} current, considering a multiplexing approach. Electronic switches S_0–S_3 are adopted to divert the current between the four devices under test (DUTs). A CompactRio board is used to control electronic switches S_0–S_3, to acquire the voltage drop V_{ce} and to communicate with the PC. Fig. 2 illustrates the typical current and voltage waveforms in one DUT. During the heating time (ON), a large current I_{dc} flows in the device, while during the cooling-down phase (OFF) a reference current I_{ref} of 50 mA is injected in the device in order to sense V_{ce}. As reported in Fig. 2(b), the $V_{ce,\mathrm{off}}$ profile is used to

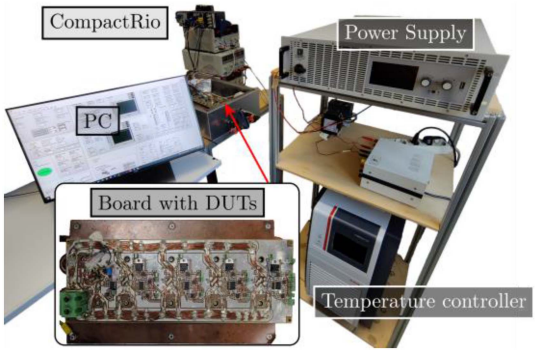

Fig. 3. Picture of the setup. The test circuit is placed on a liquid-cooled thermal plate, whose temperature is fixed by means of a temperature controller [17].

estimate the junction temperature (T_j) profile. To this purpose, the T_j vs. V_{ce} characteristic at $I_{\rm ref} = 50$ mA is first derived by means of a source measure unit and with the device placed at controlled temperature in an oven. Therefore, a temperature sensitive electrical parameter (TSEP) method is used to derive the temperature profile [33], [34]. The inset of Fig. 2(b) shows the result of the TSEP methodology. The profile starts with a maximum junction temperature $T_{j,\max}$, arising from the heating phase, and approaches to a minimum value $T_{j,\min}$ at the end of the cooling-down phase. The temperature cycling is defined as $\Delta T_j = T_{j,\max} - T_{j,\min}$. According to Fig. 2, the experimental activity has been carried out considering a periodicity of 2.5 s on four samples, hence leading to $t_{\rm on} = 0.625$ s and $t_{\rm off} = 1.875$ s, being $t_{\rm on}$ and $t_{\rm off}$ the duration of ON and OFF phases, respectively. According to [33] and [34], the selected value of $t_{\rm on}$ allows for an accurate temperature estimation when a TSEP method is considered.

As reported in Fig. 1, a bypass transistor can be adopted to sustain the $I_{\rm dc}$ current. When a DUT fails, the corresponding switch must be permanently opened and the switch S_4 is enabled in order to maintain the same $t_{\rm on}$ and $t_{\rm off}$ values on the remaining DUTs.

A picture of the experimental setup is reported in Fig. 3. The custom board, including the DUTs, is mounted on a liquid-cooled thermal plate. A thermal controller, Julabo Presto A40, is then adopted to control the temperature of the thermal plate. DUTs are placed on the back side of the custom board and are in contact with the thermal plate. The average junction temperature can be estimated as follows:

$$T_{j,\rm av} = T_{\rm ref} + R_{\rm th,jh}\, P_{\rm av} \tag{1}$$

where $P_{\rm av}$ is the average power dissipated in the DUTs, $R_{\rm th,jh}$ is the thermal resistance between the junction of the DUT and the thermal plate, and $T_{\rm ref}$ is the temperature of the thermal plate, being fixed by the temperature controller. Hence, for each experiment the $T_{\rm ref}$ is properly tuned in order to achieve the desired $T_{j,\rm av}$. It is worth noting that the $R_{\rm th,jh}$ value of a DUT is also influenced by adjacent devices (mutual heating effects). Hence, when a DUT fails and is then permanently turned-off, small changes of T_j are observed in adjacent DUTs. This effect is compensated by properly modifying the T_{ref} value. However, a transient effect may be visible in T_j and V_{ce} profiles.

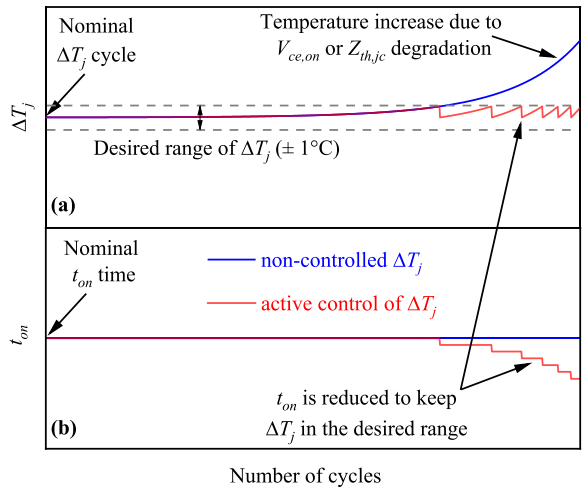

Fig. 4. Schematic representation of the different methodologies adopted for power cycling tests. In the case of "non-controlled ΔT_j" approach, the temperature swing, obtained by means of a constant heating current, deviates from the nominal value (a) because of $V_{ce,\rm on}$ or $Z_{\rm th}$ degradation. The "active control of ΔT_j" allows limiting the temperature increase by dynamically reducing the $t_{\rm on}$ time (b).

DUTs used for experiments are commercial insulated gate bipolar transistor (IGBT) with TO-247 package, with a maximum pulsed current of 120 A, a rated voltage of 650 V, and a maximum junction temperature of 175 °C. The gate of DUTs is biased with a constant dc voltage of 15 V.

The state-of-health of DUTs, subjected to power cycling stress, is estimated by monitoring the junction-to-case thermal impedance ($Z_{\rm th,jc}$) and the V_{ce} voltage at the end of the ON phase ($V_{ce,\rm on}$). The failure event is determined by an increase of $Z_{\rm th,jc}$ by 20% or $V_{ce,\rm on}$ by 5% [2]. For each power cycling condition, this work aims at analyzing the statistics of failure events. For this reason, 12 samples are tested under the same conditions.

As far as power cycling tests are concerned, different methodologies can be adopted to obtain the desired junction temperature cycling [35], [36], [37], [38]. In this work, the considered approaches are: "non-controlled ΔT_j" and "active control of ΔT_j." Details are reported in Section II-B.

B. Methodologies Adopted for Power Cycling Tests

1) Non-controlled $\Delta T_{\rm j}$*:* The power cycling tests, as discussed in Section II-A, allows achieving the desired ΔT_j by properly selecting the heating current $I_{\rm dc}$ and the heating time $t_{\rm on}$. This type of calibration is performed at the beginning of the experiment. In the case of "non-controlled ΔT_j" approach, $I_{\rm dc}$ and $t_{\rm on}$ are kept constant for the entire experiment.

As reported in Fig. 4 (blue curves), the actual ΔT_j value is not constant over the device lifetime. In fact, in the wear-out region, the device is subjected to a degradation (increase) of the thermal impedance $Z_{\rm th,jc}$ or voltage drop $V_{ce,\rm on}$. As a consequence, the internal temperature of the device increases. The ΔT_j value is a crucial parameter in determining the lifetime of power components [39]. Its increase causes a faster degradation, leading to a lower number of cycles to failure.

TABLE I
LIST OF EXPERIMENTS UNDER NON-CONSTANT ΔT_j STRESS

N range (x 10^3)	0-6	6-10	10-14	14-15	15-EoL
Test 1	140°C	120°C			
Test 2	140°C		120°C		
Test 3	120°C			140°C	
Test 4	120°C				140°C

2) Active Control of ΔT_j*:* In order to keep the ΔT_j value actually constant, or within a limited range of variation, the "active control of ΔT_j" is adopted. As shown in Fig. 4 (red curves), the increase of temperature (due to the wear-out phenomenon) is compensated by reducing the heating time of the DUT. More specifically, a hysteretic control is considered in this work. The hysteresis thresholds are ±1 °C with respect to the reference ΔT_j value. Hence, every time the ΔT_j value is out of the thresholds, the t_{on} time is reduced, or eventually increased. In this work, the change of t_{on} is limited to 30% with respect to the initial value. It is worth noting that the heating time is also a parameter affecting the lifetime of power components, even if to a lesser degree with respect to ΔT_j. Hence, it is important to avoid significant changes of t_{on} during the test.

This method is applied to all four devices mounted on the test board. As a consequence, the sum of all t_{on} times could be different (lower) with respect to the periodicity of the control signals. In this case, the bypass transistor (see Fig. 1) is activated, for a limited time, in order to warranty a constant periodicity of power cycling tests.

3) Non-Constant Cumulative Stress: Regardless of the previously discussed methods being adopted to control ΔT_j, this work aims at evaluating the case of non-constant power cycling tests, in which the ΔT_j is changed on purpose during the test. This is achieved by modifying the I_{dc} value during the power cycling test.

Non-constant power cycling tests are designed by considering the combination of two specific ΔT_j values: 120 and 140 °C. The detailed list of tests is reported in Table I. It can be observed that non-constant power cycling tests foresee a different order of ΔT_j stresses and a different switching point (expressed as a number of cycles).

The study of the lifetime under non-constant cumulative stress requires the knowledge of the statistics of failure events occurring under constant stress conditions. The cumulative distribution function (CDF) gives the probability that a device will fail within a given number of cycles N (in order words the percentage of population expected to be failed as a function of N). The Weibull statistics is widely adopted to describe thermal/power cycling phenomena in power semiconductor devices [1]. The CDF is expressed as follows:

$$\mathrm{CDF}_{\mathrm{Weibull}} = 1 - e^{-(N/\beta)^{\alpha}} \tag{2}$$

where α is the shape parameter and β is the scale parameter. By considering the reverse function of (2), it is possible to estimate the expected number of cycles to failure at different probabilities of failure (PoFs): 10%, 25%, 50%, and 75%. In order words, this is the number of cycles at which a given percentage of a population will have failed. This kind of estimation is performed for both 120 and 140 °C constant stresses.

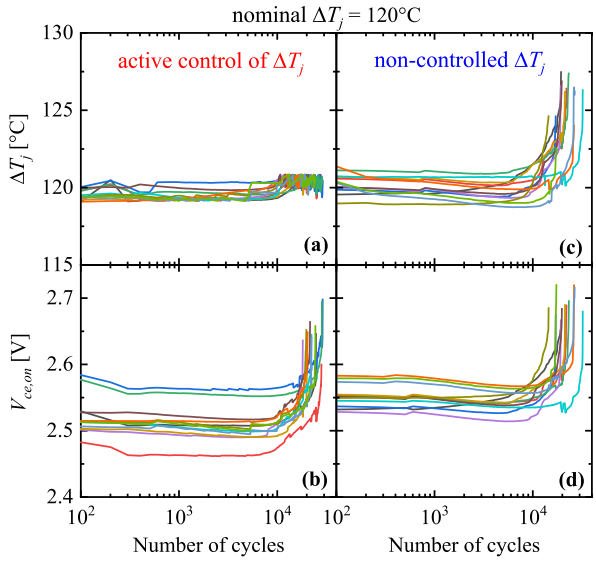

Fig. 5. Power cycling tests carried out under constant stress conditions. Temperature swing and $V_{ce,on}$ profiles are reported as a function of the number of cycles in the case of "active control of ΔT_j," (a) and (b), and in the case of "non-controlled ΔT_j," (c) and (d). Twelve samples are stressed under the same test conditions ($T_{j,min}$ = 25 °C and ΔT_j = 120 °C). The increase of $V_{ce,on}$ by 5% is considered as failure criterion.

The Miner's rule is usually adopted in order to estimate the lifetime consumption (*LC*) of devices subjected to non-constant thermal/power cycling stresses [40], [41]. Under the assumption of linear damage accumulation, the *LC* at a given y percentage of PoF is given by the following:

$$\mathrm{LC}_y = \sum_i \frac{n_i}{N_{i,y}} \tag{3}$$

where n_i is the number of cycles for the ith type of stress and $N_{i,y}$ is the expected lifetime, in terms of number of cycles, at the y percentage of PoF for the ith type of stress. Hence, $N_{i,y}$ is estimated by reversing (2) for ΔT_j = 120 °C and ΔT_j = 140 °C. *LC* represents the fraction of life consumed by the application of a non-constant power cycling stress. When LC_y reaches the value of 1, the failure occurs and the lifetime can be determined. Being a statistical event, this lifetime represents the number of cycles with y percentage of probability of failure. The data extrapolated with the Miner's rule can be then compared with experimental results arising from the application of non-constant cumulative stress.

III. RESULTS AND DISCUSSION

A. Power Cycling Tests Under Constant ΔT_j Stress

In this section, the experimental results of power cycling tests are reported, by considering constant ΔT_j values: 120 and 140 °C. In both cases, "non-controlled ΔT_j" and "active control of ΔT_j" approaches are considered for the sake of comparison. $V_{ce,on}$ and ΔT_j profiles are reported in Fig. 5 for the nominal ΔT_j = 120 °C. The adopted heating current is 63.5 A with a

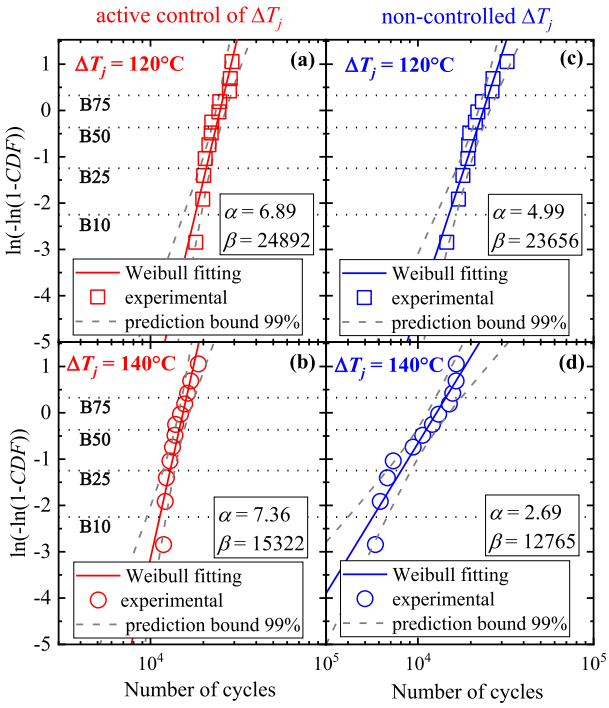

Fig. 6. Experimental cumulative distribution functions for constant $\Delta T_j = 120$ °C and $\Delta T_j = 140$ °C. Results arising from both techniques, "active control of ΔT_j" and "non-controlled ΔT_j," are reported. Experimental data are fitted assuming a Weibull distribution. Prediction bounds (99%) are also included in the plots.

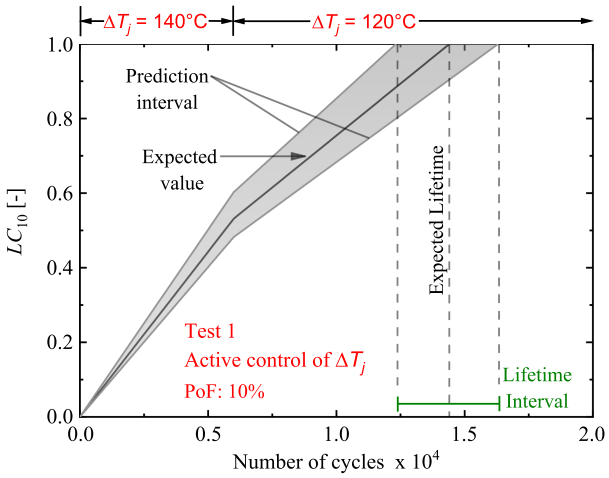

Fig. 7. Application of the Miner's rule for the determination of the lifetime in the case of non-constant stress (Test 1 of Table I). Lifetime consumption (LC) is calculated according to (3), by considering the expected number of cycles estimated in Fig. 6 for a PoF of 10%. The prediction interval arises from the prediction bound of Fig. 6.

maximum variation of ±0.5 A, with $T_{j,\min} = 25$ °C. In the case of "active control of ΔT_j," the temperature swing is kept constant to the nominal value of 120 °C, within the hysteresis threshold of 1 °C [see Fig. 5(a)]. The $V_{ce,on}$ profile, reported in Fig. 5(b), is initially flat, while it sharply increases close to the end of life of the components. In all 12 experiments the failure is determined by an increase of $V_{ce,on}$ by 5%, while $Z_{th,jc}$ is almost unchanged (not shown here). On the other hand,

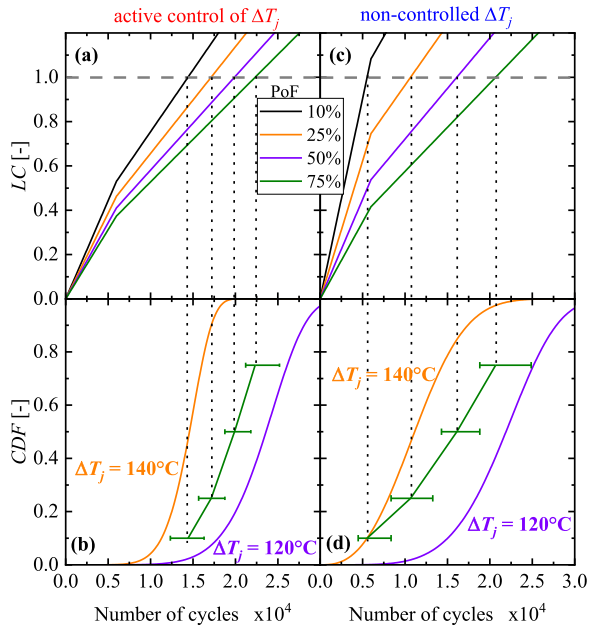

Fig. 8. Combined non-constant power cycling stress (Test 1 of Table I) for both "active control of ΔT_j" (left column) and "non-controlled ΔT_j" (right column). Lifetime consumption is reported in (a) and (c) considering different probabilities of failure. CDFs arising from the application of the Miner's rule are as reported in (b) and (d), along with prediction bounds. Weibull fittings for constant $\Delta T_j = 120$ °C and $\Delta T_j = 140$ °C are included in order to delimit the region in which results are expected to be found.

in the case of "non-controlled ΔT_j" approach, the temperature swing increases up to around 127 °C [see Fig. 5(c)]. Although the qualitative profile of $V_{ce,on}$ [see Fig. 5(d)] is in agreement with the one observed in the case of "active control of ΔT_j," the increase of temperature reported in Fig. 5(b) is responsible of modifications in the number of cycles to failure. In the case of $\Delta T_j = 140$ °C, an heating current of 68.5 A is adopted, with $T_{j,\min} = 25$ °C. $V_{ce,on}$ and ΔT_j profiles (not reported here) are analogous to those reported in Fig. 5.

The experimental number of cycles to failure can be adopted to build the CDF plot. By means of the Bernard formula [42], the experimental CDF is expressed as follows:

$$\mathrm{CDF}_{\mathrm{exp}}(N_k) = \frac{k - 0.3}{N_{\mathrm{tot}} + 0.4} \tag{4}$$

where N_k is the number of cycles to failure of the kth experiment (with experiments sorted in ascending order according to the number of cycles to failure) and $N_{\mathrm{tot}} = 12$ is the total number of experiments. Results are reported in Fig. 6 for both $\Delta T_j = 120$ °C and $\Delta T_j = 140$ °C and for both "non-controlled ΔT_j" and "active control of ΔT_j" approaches. Aiming at linearizing the dependence between CDF and N, the expression of (2) can be written as follows:

$$\ln(-\ln(1 - \mathrm{CDF})) = \alpha \cdot \ln(N) - \alpha \cdot \ln(\beta). \tag{5}$$

Hence, in the case of Weibull distribution, a linear fitting can be adopted to estimate both α and β parameters. Lines at specific PoFs are reported in Fig. 6 and are labeled B10, B25, B50, and

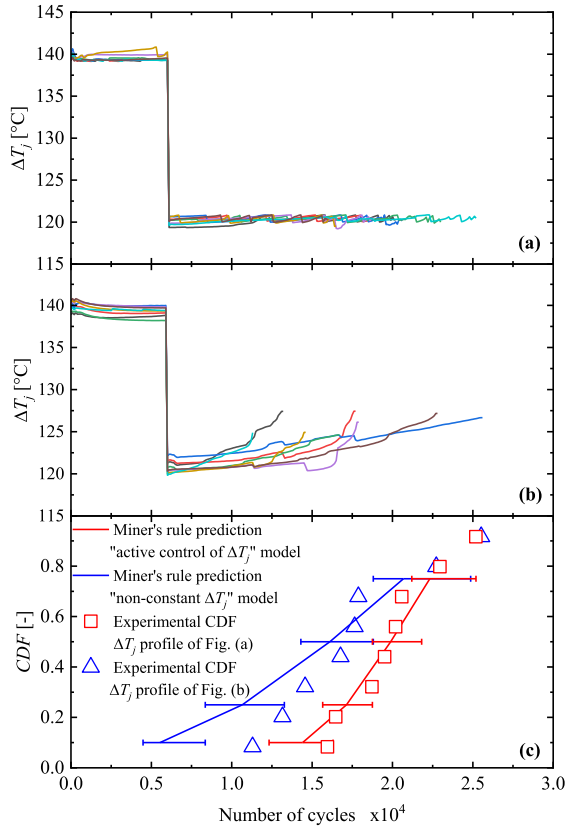

Fig. 9. Experimental non-constant ΔT_j stresses for Test 1. In (a) the temperature cycling profile is obtained by actively controlling the heating time. In (b) a constant heating current is adopted, leading an increase of temperature close to the end of life. Experimental CDFs, for both ΔT_j profiles, are reported in (c) and compared with those calculated according to the Miner's rule (see Fig. 8).

B75. In general, the adoption of "active control of ΔT_j" approach leads to a larger number of cycles to failure for a given PoF with respect to the "non-controlled ΔT_j" approach. In the latter case, according to [43], a positive feedback relationship between the wire bonds degradation and ΔT_j leads to lower lifetimes.

CDFs, estimated in the case of "active control of ΔT_j" approach, exhibit a similar shape parameter α, while the change of the stress level leads to a modification of the scale parameter β. On the other hand, the adoption of "non-controlled ΔT_j" approach leads to a statistic in which the shape parameter α is significantly reduced in the case of $\Delta T_j = 140$ °C. It is possible that during the degradation phase the non-controlled increase of temperature can cause some early failures, hence modifying the α parameter of the distribution.

B. *Power Cycling Tests Under Non-Constant* ΔT_j *Stress*

In the case of non-constant ΔT_j stress, Miner's rule is adopted for the lifetime estimation. The case of Test 1 (as illustrated in Table I) is reported in Fig. 7. Non-constant stress is defined as: 6000 cycles at $\Delta T_j = 140$ °C and the remaining cycles at $\Delta T_j = 120$ °C, with $T_{j,\min} = 25$ °C. According to (3), the lifetime consumption is calculated by considering the expected number of cycles at $\Delta T_j = 120$ °C and $\Delta T_j = 140$ °C. These values can be directly derived from Fig. 6(a) and (b) (active control of ΔT_j) for the given PoF (10%). However, the CDFs of Fig. 6 are defined within given prediction bounds with a level of certainty of 99%. Consequently, the *LC* profile is also known in a prediction interval, as reported in Fig. 7. The lifetime is then calculated as the number of cycles leading to $LC = 1$. Overall, a lifetime interval can be estimated, arising from the limited statistics in the experimental activity.

For the sake of comparison, the analysis of Test 1 is then carried out by considering lifetime models derived with both "non-controlled ΔT_j" and "active control of ΔT_j" approaches and for the probability of failure ranging from 10% to 75%. The application of Miner's rule for both cases is reported in Fig. 8. The lifetime consumption is estimated in Fig. 8(a) and (c) at different PoF. By using these pairs of values, i.e., the number of cycles to failure and the PoF, a CDF can be predicted according to Miner's rule [see Fig. 8(b) and (d)]. Although both predicted CDFs are included in the range of constant stresses ($\Delta T_j = 120$ °C and $\Delta T_j = 140$ °C), the adoption of lifetime models

TABLE II
EXPERIMENTAL LIFETIME VERSUS LIFETIME PREDICTION ACCORDING TO MINER'S RULE (3)

	PoF [%]	Exp. # cycles	Estimated with (3) [%]	Prediction bound [%]
Test 1 (active control of ΔT_j)	10	16028	111.22	[98.30; 130.03]
	25	17373	101.36	[92.65; 110.95]
	50	19858	99.84	[91.02; 105.90]
	75	22006	98.58	[87.35; 103.78]
Test 1 (non-controlled ΔT_j)	10	11506	208.81	[150.77; 289.21]
	25	13723	128.79	[107.62; 178.83]
	50	17210	106.86	[93.24; 122.64]
	75	20790	100.51	[85.00; 113.71]

Note: Lifetime estimated with (3) and prediction bound are expressed as a percentage of the experimental number of cycles to failure. Active "control of ΔT_j" approach is compared with the case of "non-controlled ΔT_j" approach.

TABLE III
EXPERIMENTAL LIFETIME VERSUS LIFETIME PREDICTION ACCORDING TO MINER'S RULE (3)

active control of ΔT_j	PoF [%]	Exp. # cycles	Estimated with (3) [%]	Prediction bound [%]
Test 1	10	16028	111.22	[98.30; 130.03]
	25	17373	101.36	[92.65;110.95]
	50	19858	99.84	[91.02; 105.90]
	75	22006	98.58	[87.35; 103.78]
Test 2	10	11228	93.19	[80.74; 112.79]
	25	13374	90.87	[81.93; 101.62]
	50	16740	96.14	[86.10; 102.55]
	75	18436	93.08	[81.04; 98.31]
Test 3	10	16013	97.13	[90.51; 105.32]
	25	17166	94.22	[89.30; 99.06]
	50	19884	99.76	[94.06; 103.44]
	75	21089	98.43	[90.81; 101.65]
Test 4	10	16843	100.50	[93.15; 117,39]
	25	16994	91.49	[86.80; 97.97]
	50	19300	95.50	[88.58; 98.97]
	75	19972	91.19	[81.49; 95.89]

Note: Lifetime estimated with (3) and prediction bound are expressed as a percentage of the experimental number of cycles to failure. Different non-constant power cycling test conditions are considered in the case of "active control of ΔT_j."

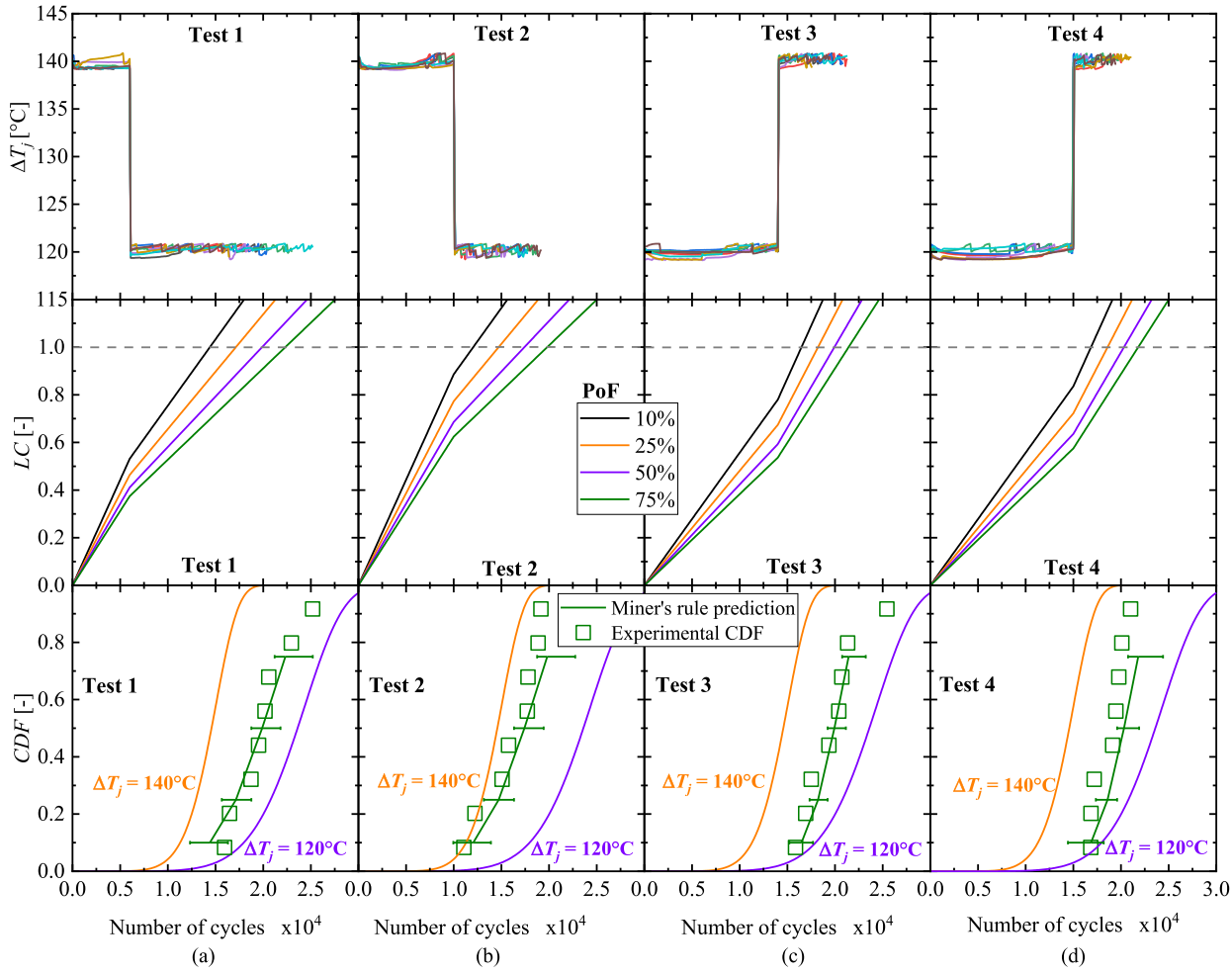

Fig. 10. Combined non-constant power cycling stress in the case of "active control of ΔT_j" for different test conditions (as reported in Table I). In all considered cases, the experimental CDF is within the prediction bound of the Miner's rule prediction.

calibrated with a "non-controlled ΔT_j" approach leads to higher probability of failure (under non-constant stress).

Experimental non-constant ΔT_j stresses are reported in Fig. 9 in the case of Test 1. In Fig. 9(a), ΔT_j profiles were obtained by actively controlling t_{on} and hence exactly matching the conditions of Test 1 (see Table I). This is the most appropriate profile to consider, since the only available lifetime models are those for $\Delta T_j = 120$ °C and $\Delta T_j = 140$ °C. For the sake of comparison, in Fig. 9(b) ΔT_j profiles were generated by only controlling the heating current, hence an uncontrolled temperature increase close to the end of life is observed. In Fig. 9(c), by considering the CDF calculated on the basis of models calibrated with the "active control of ΔT_j" methodology, the application of the Miner's rule leads to a lifetime prediction being in a very good agreement with the experimental CDF deriving from the tests of Fig. 9(a). As reported in Table II, the experimental number of cycles to failure is always included in the prediction interval (associated to the Miner's rule estimation) for the full range of PoFs. In the case of "non-controlled ΔT_j" approach, the application of Miner's rule leads to a lifetime prediction which is accurate in the case of large PoFs, while at low PoF the experimental results differ from the calculated values (they are even outside of the prediction intervals). Considering the non-constant stress profile of Fig. 9(b) (in which the stress methodology is analogous to the one adopted for the calibration of lifetime models) the difference between the Miner's prediction and the experimental CDF decreases but it is still relevant in the case of PoF close to 10%. The error around PoF $=$ 10% can be explained by considering CDFs at constant stress reported in Fig. 6. More specifically, in Fig. 6(d) the number of cycles to failure for $\Delta T_j = 140$ °C is very low in the case of PoF $=$ 10%. As discussed in Section III-A, this is probably due to the positive feedback relationship between the wire bonds degradation and ΔT_j, possibly leading to the premature failure of samples in which the thermo-mechanical stress is not kept constant. As a result, the application of the (3) in the case of combined 140 °C/120 °C stress leads to an underestimation of the lifetime with respect to the experimental value at PoF $=$ 10%.

According to the analysis reported in Fig. 9 and Table II, the way in which accelerated lifetime tests are performed can have an impact on the accuracy of the linear damage accumulation theory. On one hand, if lifetime models are calibrated by means of accelerated tests with "active control of ΔT_j," the thermo-mechanical stress can be considered constant, since ΔT_j

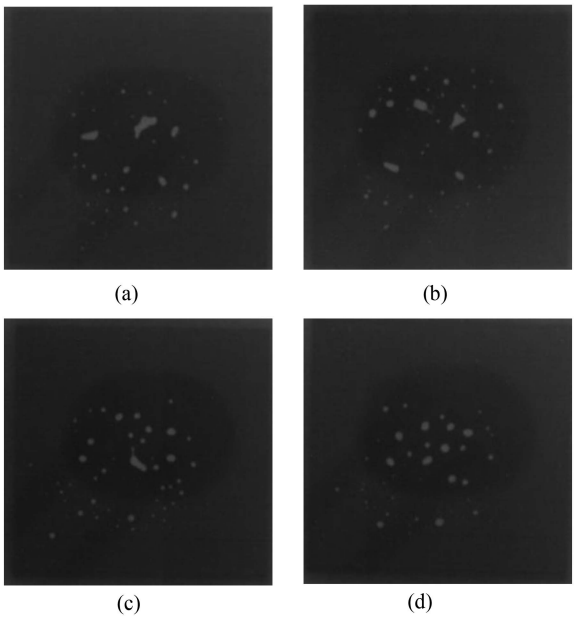

Fig. 11. X-ray images of solder joint regions taken from the back side of the component. (a) Fresh device. (b) After failure—$\Delta T_j = 120$ °C with "active control of ΔT_j." (c) After failure—$\Delta T_j = 120$ °C with "non-controlled ΔT_j." (d) After failure—Test 1. Voids can be observed in all samples at the Si/copper tab interface.

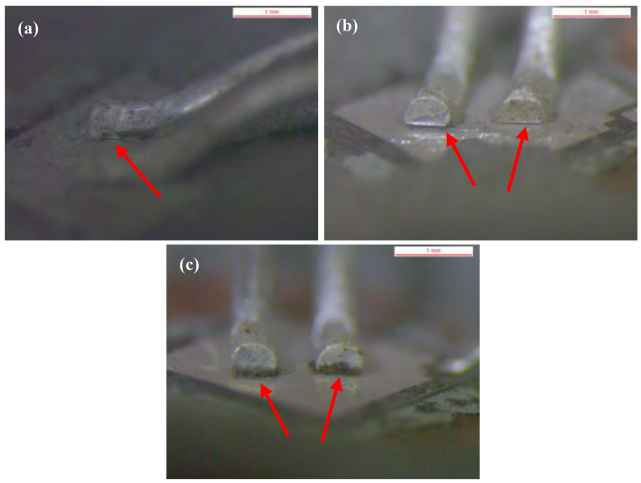

Fig. 12. Microscope images of wire bonds after power cycling failures. (a) $\Delta T_j = 120$ °C with "active control of ΔT_j." (b) $\Delta T_j = 120$ °C with "non-controlled ΔT_j." (c) Test 1. Red arrows indicate the localization of the crack formation.

is fixed at the nominal value. Consequently, Miner's rule gives an accurate prediction when the considered stress is a combination of the stresses at constant ΔT_j. On the other hand, during the calibration of lifetime models based on a "non-controlled ΔT_j" approach, power devices are subjected to a temperature cycling exceeding the nominal ΔT_j value. Therefore, the effective ΔT_j value to be considered for the lifetime modeling purpose should be higher. When applying Miner's rule for a given (non-constant) temperature profile, the adopted lifetime model is based on the nominal ΔT_j value rather than the effective ΔT_j value. Hence, some inaccuracies are introduced in the lifetime estimation.

The "active control of ΔT_j" approach is extensively verified in all the test conditions reported in Table I and the results are illustrated in Fig. 10. The different conditions foresee the same ΔT_j stresses (120 and 140 °C), but with different orders and switching points. Therefore, Miner's rule predictions can be again estimated from the results of Fig. 6. As illustrated in Fig. 10 the experimental CDFs are always well aligned with the application of the Miner's rule. The maximum error, which is reported in Table III, is in the order of 10%, which typically falls in the prediction bound calculated for the lifetime estimation. Therefore, we can conclude that the application of Miner's rule allows accurately calculating the number of cycles to failure at any PoF.

C. Analysis of Degradation Mechanisms

Device under tests considered in this article are discrete IGBTs in TO-247 package. They are characterized by a typical lead-frame substrate and solderable pins as terminal contacts. Discrete devices are encapsulated in a transfer mold compound based on an epoxy resin [44].

In order to observe the presence of stress in the solder joint region, X-ray images are captured by means of an EasyTom tomograph. The fresh sample, reported in Fig. 11(a), shows some voids at the interface between the silicon die and the copper tab, which can be ascribed to the manufacturing process [21], [23], [25]. Similarly, devices subjected to power cycling (both constant and non-constant temperature cycling) exhibit some voids, but no signs of delamination can be found in Fig. 11(b), (c), or (d). It is worth noting that the solder joint has a significantly larger volume, with respect to wire bonds, with a consequent higher thermal time constant. For this reason, the solder joint fatigue typically occurs when considering a longer heating time than the value considered in this article ($t_{\rm on} = 0.625$ s) [8].

The packages of some samples have been opened for the inspection of wire bonds. As reported in Fig. 12, in all considered cases (both constant and non-constant temperature cycling, both "active control of ΔT_j" and "non-controlled ΔT_j") the formation of a crack at the Al/Si interface is visible in the images acquired through a Leica MS5 microscope. Therefore, according to this study, the discussion about the applicability of the LDA theory is related to the wire bonds degradation mechanism. It is worth mentioning that Miner's rule can be considered only if a single failure mode occurs in the component [25].

The analysis of degradation mechanisms is in agreement with the electrical wear-out of the components. In fact, as reported in Fig. 5, the failure events are associated to an increase of $V_{ce,\rm on}$, while $Z_{\rm th,}jc$ is basically unchanged [45].

IV. Conclusion

In this article, different methodologies are considered for the accelerated lifetime testing of TO-247 IGBT devices subjected to power cycling stress, aimed at understanding, from an academic point of view, differences in the lifetime estimation under non-constant stress. More specifically, the "active control of

ΔT_j" approach consists in dynamically modulating the heating time in order to keep a constant ΔT_j. In this case, the analysis of an arbitrary temperature profile by means of Miner's rule, allows to predict the CDF in very good agreement with experimental tests (under non-constant stress). Hence, the applicability of the linear damage accumulation rule is confirmed under the hypothesis that lifetime models are calibrated with an "active control of ΔT_j" approach. However, guidelines for the qualification of power devices, such as [46], typically do not allow for modifications of the heating time during the power cycling test. This approach is referred to as "non-controlled ΔT_j" method in this article, since the application of a constant heating current leads to a change of the temperature swing during the test (due to the modification of self-heating effects). In this case, the application of the Miner's rule for an arbitrary mission profile can lead to less accurate results, but still in the prediction bounds if large probabilities of failure are considered.

ACKNOWLEDGMENT

The authors would like to thank the staff of the Laboratory of Computed Tomography and of the Laboratory of Metallurgy at DTG, University of Padova, for useful discussions and for the support in the experimental failure analysis.

REFERENCES

[1] R. Amro, J. Lutz, and A. Lindemann, "Power cycling with high temperature swing of discrete components based on different technologies," in *Proc. IEEE 35th Annu. Power Electron. Spec. Conf.*, 2004, vol. 4, pp. 2593–2598, doi: 10.1109/PESC.2004.1355239.

[2] J. Lutz, H. Schlangenotto, U. Scheuermann, and R. De Doncker, *Semiconductor Power Devices*, vol. 4. Berlin, Germany: Springer, 2011.

[3] M. Demir, G. Kahramanoglu, and A. Bekir Yildiz, "Importance of reliability for power electronic circuits, case study: Inrush current test and calculating of fuse melting point," in *Proc. IEEE Int. Power Electron. Motion Control Conf.*, 2016, pp. 830–834, doi: 10.1109/EPEPEMC.2016.7752101.

[4] S. Yang, D. Xiang, A. Bryant, P. Mawby, L. Ran, and P. Tavner, "Condition monitoring for device reliability in power electronic converters: A review," *IEEE Trans. Power Electron.*, vol. 25, no. 11. pp. 2734–2752, Nov. 2010.

[5] M. Held, P. Jacob, G. Nicoletti, P. Scacco, and M. H. Poech, "Fast power cycling test for IGBT modules in traction application," in *Proc. IEEE Int. Conf. Power Electron. Drive Syst.*, 1997, vol. 1, pp. 425–430, doi: 10.1109/peds.1997.618742.

[6] A. Otto and S. Rzepka, "Lifetime modelling of discrete power electronic devices for automotive applications," in *Proc. IEEE Automot. Electron.-Beitrage der 10. GMM-Fachtagung*, 2019, pp. 105–110.

[7] L. R. GopiReddy, L. M. Tolbert, and B. Ozpineci, "Power cycle testing of power switches: A literature survey," *IEEE Trans. Power Electron.*, vol. 30, no. 5, pp. 2465–2473, May 2015.

[8] S. Dusmez, S. H. Ali, M. Heydarzadeh, A. S. Kamath, H. Duran, and B. Akin, "Aging precursor identification and lifetime estimation for thermally aged discrete package silicon power switches," *IEEE Trans. Ind. Appl.*, vol. 53, no. 1, pp. 251–260, Jan./Feb. 2017.

[9] M. Brincker, K. B. Pedersen, P. K. Kristensen, and V. N. Popok, "Effects of thermal cycling on aluminum metallization of power diodes," *Microelectron. Reliab.*, vol. 55, no. 9/10, pp. 1988–1991, Aug. 2015, doi: 10.1016/j.microrel.2015.06.005.

[10] A. Otto, S. Rzepka, and B. Wunderle, "Investigation of active power cycling combined with passive thermal cycles on discrete power electronic devices," *J. Electron. Packag. Trans. ASME*, vol. 141, no. 3, 2019, Art. no. 31012, doi: 10.1115/1.4043646.

[11] R. Bayerer, T. Herrmann, T. Licht, J. Lutz, and M. Feller, "Model for power cycling lifetime of IGBT modules–Various factors influencing lifetime," in *Proc. IEEE 5th Int. Conf. Integr. Power Electron. Syst., Proc.*, 2008, pp. 37–42.

[12] U. Scheuermann and R. Schmidt, "A new lifetime model for advanced power modules with sintered chips and optimized Al wire bonds," in *Proc. PCIM Europe Conf. Proc.*, 2013, pp. 810–817.

[13] M. Hernes, S. D'Arco, A. Antonopoulos, and D. Peftitsis, "Failure analysis and lifetime assessment of IGBT power modules at low temperature stress cycles," *IET Power Electron.*, vol. 14, no. 7, pp. 1271–1283, 2021, doi: 10.1049/pel2.12083.

[14] S. H. Ali, M. Heydarzadeh, S. Dusmez, X. Li, A. S. Kamath, and B. Akin, "Lifetime estimation of discrete IGBT devices based on Gaussian process," *IEEE Trans. Ind. Appl.*, vol. 54, no. 1, pp. 395–403, Jan./Feb. 2018.

[15] S. Pu, F. Yang, B. T. Vankayalapati, and B. Akin, "Aging mechanisms and accelerated lifetime tests for SiC MOSFETs: An overview," *IEEE J. Emerg. Sel. Top. Power Electron.*, vol. 10, no. 1, pp. 1232–1254, Feb. 2022.

[16] H. Luo, F. Iannuzzo, F. Blaabjerg, M. Turnaturi, and E. Mattiuzzo, "Aging precursors and degradation effects of SiC-MOSFET modules under highly accelerated power cycling conditions," in *Proc. IEEE Energy Convers. Congr. Expo.*, 2017, vol. 2017, pp. 2506–2511, doi: 10.1109/ECCE.2017.8096478.

[17] A. Vaccaro, P. Magnone, A. Zilio, and P. Mattavelli, "Predicting lifetime of semiconductor power devices under power cycling stress using artificial neural network," *IEEE J. Emerg. Sel. Topics Power Electron.*, to be published, doi: 10.1109/JESTPE.2022.3194189.

[18] K. Ma, U. M. Choi, and F. Blaabjerg, "Prediction and validation of wear-out reliability metrics for power semiconductor devices with mission profiles in motor drive application," *IEEE Trans. Power Electron.*, vol. 33, no. 11, pp. 9843–9853, Nov. 2018.

[19] L. Ceccarelli, R. M. Kotecha, A. S. Bahman, F. Iannuzzo, and H. A. Mantooth, "Mission-profile-based lifetime prediction for a SiC MOSFET power module using a multi-step condition-mapping simulation strategy," *IEEE Trans. Power Electron.*, vol. 34, no. 10, pp. 9698–9708, Oct. 2019.

[20] D. Zhou, H. Wang, F. Blaabjerg, S. K. Kaer, and D. Blom-Hansen, "Real mission profile based lifetime estimation of fuel-cell power converter," in *Proc. IEEE 8th Int. Power Electron. Motion Control Conf.*, 2016, pp. 2798–2805, doi: 10.1109/IPEMC.2016.7512741.

[21] U. M. Choi, K. Ma, and F. Blaabjerg, "Validation of lifetime prediction of IGBT modules based on linear damage accumulation by means of superimposed power cycling tests," *IEEE Trans. Ind. Electron.*, vol. 65, no. 4, pp. 3520–3529, Apr. 2018.

[22] L. R. GopiReddy, L. M. Tolbert, B. Ozpineci, and J. O. P. Pinto, "Rainflow algorithm-based lifetime estimation of power semiconductors in utility applications," *IEEE Trans. Ind. Appl.*, vol. 51, no. 4, pp. 3368–3375, Jul./Aug. 2015.

[23] G. Zeng, L. Borucki, O. Wenzel, O. Schilling, and J. Lutz, "First results of development of a lifetime model for transfer molded discrete power devices," in *Proc. IEEE Int. Exhib. Conf. Power Electron., Intell. Motion, Renewable Energy Energy Manage.*, 2018, pp. 706–713.

[24] U. Scheuermann and U. Hecht, "Power cycling lifetime of advanced power modules for different temperature swings," in *Proc. PCIM Nuremb.*, 2002, pp. 59–64. [Online]. Available: http://scholar.google.com/scholar?hl=en&btnG=Search&q=intitle:Power+Cycling+Lifetime+of+Advanced+Power+Modules+for+Different+Temperature+Swings#0

[25] G. Zeng, C. Herold, T. Methfessel, M. Schafer, O. Schilling, and J. Lutz, "Experimental investigation of linear cumulative damage theory with power cycling test," *IEEE Trans. Power Electron.*, vol. 34, no. 5, pp. 4722–4728, May 2019.

[26] Z. Khatir, S. H. Tran, A. Ibrahim, R. Lallemand, and N. Degrenne, "Effect of load sequence interaction on bond-wire lifetime due to power cycling," *Sci. Rep.*, vol. 11, no. 1, 2021, Art. no. 5601, doi: 10.1038/s41598-021-84976-2.

[27] H. Qi, M. Osterman, and M. Pecht, "Plastic ball grid array solder joint reliability for avionics applications," *IEEE Trans. Compon. Packag. Technol.*, vol. 30, no. 2, pp. 242–247, Jun. 2007.

[28] K. Upadhyayula and A. Dasgupta, "Incremental damage superposition approach for reliability of electronic interconnects under combined accelerated stresses," in *Proc. ASME Int. Mech. Eng. Congr. Exposit.*, Dallas, USA, 1997.

[29] A. Perkins and S. K. Sitaraman, "A study into the sequencing of thermal cycling and vibration tests," in *Proc. Electron. Compon. Technol. Conf.*, 2008, pp. 584–592, doi: 10.1109/ECTC.2008.4550032.

[30] C. Basaran and R. Chandaroy, "Thermomechanical analysis of solder joints under thermal and vibrational loading," *J. Electron. Packag. Trans. ASME*, vol. 124, no. 1, pp. 60–66, 2002, doi: 10.1115/1.1400752.

[31] D. Ghaderi, M. Pourmahdavi, V. Samavatian, O. Mir, and M. Samavatian, "Combination of thermal cycling and vibration loading effects on the fatigue life of solder joints in a power module," in *Proc. Inst. Mech. Engineers, Part L: J. Mater.: Des. Appl.*, vol. 233, no. 9, pp. 1753–1763, 2019, doi: 10.1177/1464420718780525.
[32] A. Vaccaro and P. Magnone, "Analysis of thermal cycling effects in power devices under non-constant cumulative stress," in *Proc. IEEE Appl. Power Electron. Conf. Expo.*, 2022, pp. 330–335, doi: 10.1109/APEC43599.2022.9773598.
[33] F. Nehr and U. Scheuermann, "Consequences of temperature imbalance for the interpretation of virtual junction temperature provided by the VCE(T)-method," in *Proc. Int. Exhib. Conf. Power Electron., Intell. Motion, Renewable Energy Energy Manage.*, 2022, pp. 627–634, doi: 10.30420/565822086.
[34] C. Herold, J. Franke, R. Bhojani, A. Schleicher, and J. Lutz, "Requirements in power cycling for precise lifetime estimation," *Microelectron. Reliab.*, vol. 58, pp. 82–89, 2016, doi: 10.1016/j.microrel.2015.12.035.
[35] G. Zeng, F. Wenisch-Kober, and J. Lutz, "Study on power cycling test with different control strategies," *Microelectron. Reliab.*, vol. 88–90, pp. 756–761, 2018, doi: 10.1016/j.microrel.2018.07.088.
[36] U. M. Choi, S. Jorgensen, and F. Blaabjerg, "Advanced accelerated power cycling test for reliability investigation of power device modules," *IEEE Trans. Power Electron.*, vol. 31, no. 12, pp. 8371–8386, Dec. 2016.
[37] U. Scheuermann and S. Schuler, "Power cycling results for different control strategies," *Microelectron. Reliab.*, vol. 50, no. 9/11, pp. 1203–1209, 2010, doi: 10.1016/j.microrel.2010.07.135.
[38] Z. Sarkany, A. Vass-Varnai, and M. Rencz, "Comparison of different power cycling strategies for accelerated lifetime testing of power devices," in *Proc. IEEE 5th Electron. Syst.-Integration Technol. Conf.*, 2014, pp. 1–5, doi: 10.1109/ESTC.2014.6962833.
[39] R. Schmidt, F. Zeyss, and U. Scheuermann, "Impact of absolute junction temperature on power cycling lifetime," in *Proc. IEEE 15th Eur. Conf. Power Electron. Appl.*, 2013, pp. 1–10, doi: 10.1109/EPE.2013.6631835.
[40] H. Huang and P. A. Mawby, "A lifetime estimation technique for voltage source inverters," *IEEE Trans. Power Electron.*, vol. 28, no. 8, pp. 4113–4119, Aug. 2013.
[41] M. A. Miner, "Cumulative damage in fatigue," *J. Appl. Mech.*, vol. 12, no. 3, pp. A159–A164, 1945, doi: 10.1115/1.4009458.
[42] S. N. Luko, "A review of the weibull distribution and selected engineering applications," *SAE Trans.*, vol. 108, pp. 398–412, 1999. [Online]. Available: http://www.jstor.org/stable/44723063
[43] S. H. Tran et al., "Constant δt j power cycling strategy in DC mode for top-metal and bond-wire contacts degradation investigations," *IEEE Trans. Power Electron.*, vol. 34, no. 3, Mar. 2019.
[44] A. Otto, R. Dudek, R. Döring, and S. Rzepka, "Investigating the mold compounds influence on power cycling lifetime of discrete power devices," in *Proc. IEEE Int. Exhib. Conf. Power Electron., Intell. Motion, Renewable Energy Energy Manage.*, 2019, pp. 479–486.
[45] L. Josef, "IGBT-modules : Design for reliability IGBT-modules : Design for reliability," in *Proc. IEEE 13th Eur. Conf. Power Electron. Appl.*, 2016, pp. 1–3.
[46] "Qualification of power modules for use in power electronics converter units in motor vehicles," ECPE Guideline AQG 324, Rev. 03.1/2021.

Alessandro Vaccaro (Student Member, IEEE) was born in Cariati, Italy, in 1996. He received the B.S. (cum laude) and M.S. (cum laude) degrees in electronics engineering from the University of Calabria, Rende, Italy, in 2018 and 2020, respectively. He is currently working toward the Ph.D. degree in mechatronics in the University of Padova, Vicenza, Italy.

His research interests include the experimental analysis and reliability of semiconductor power devices.

Paolo Magnone (Senior Member, IEEE) received the B.S. and M.S. degrees from the University of Calabria, Rende, Italy, in 2003 and 2005, respectively, and the Ph.D. degree from the University of Reggio Calabria, Reggio Calabria, Italy, in 2009, all in electronic engineering.

In the period 2006–2008, he joined for one year the Interuniversity MicroElectronics Center (IMEC), Leuven, Belgium, within the "Advanced PROcess Technologies for Horizontal Integration" project (Marie Curie Actions), where he worked on parameters extraction and matching analysis of FinFET devices. From 2009 to 2010, he was a Postdoctoral Researcher with the University of Calabria. From 2010 to 2014, he was with the Advanced Research Center on Electronic Systems for Information and Communication Technologies "E. De Castro" (ARCES), University of Bologna, Italy. In 2014, he was appointed Associate Professor of electronics at the University of Padova, Italy. His current research interests include the electrical characterization and modeling of semiconductor devices and circuits for power applications.

Dr. Magnone serves as an Editor for IEEE JESTPE.